THE JOURNAL OF BIOLOGICAL CHEMISTRY VOL. 292, NO. 15, pp. 6381–6388, April 14, 2017

Role of glycine 221 in catalytic activity of hyaluronan-binding protein 2

Received for publication, September 13, 2016, and in revised form, February 25, 2017 Published, JBC Papers in Press, February 27, 2017, DOI 10.1074/jbc.M116.757849

Fabian Stavenuiter[‡], **Eduard H. T. M. Ebberink**[‡], **Koen Mertens**[‡§], **and Alexander B. Meijer**[‡§1]

From the [‡]*Department of Plasma Proteins, Sanquin Research, 1066 CX Amsterdam, The Netherlands and the* [§]*Department of Pharmaceutics, Utrecht Institute for Pharmaceutical Sciences, Utrecht University, 3584 CG Utrecht, The Netherlands*

Edited by Norma Allewell

HABP2 (hyaluronan-binding protein 2) is a Ca^{2+}-dependent serine protease with putative roles in blood coagulation and fibrinolysis. A G221E substitution, known as the Marburg I polymorphism, reportedly affects HABP2 function and has been associated with increased risk for cardiovascular disease. However, the importance of Gly-221 for HABP2 activity is unclear. Here, we used G221E, G221A, and G221S mutants to assess the role of Gly-221 in HABP2 catalysis. The G221E variant failed to activate the single-chain urokinase-type plasminogen activator, and the G221A and G221S variants displayed moderately reduced single-chain urokinase-type plasminogen activator activation. Activity toward the peptide substrate S-2288 was markedly decreased in all HABP2 variants, with G221E being the most defective and G221A being the least defective. In the absence of Ca^{2+}, S-2288 cleavage by wild-type HABP2 was Na^+-dependent, with K_m decreasing from 3.0 to 0.6 mM upon titration from 0 to 0.3 M Na^+. In the presence of 5 mM Ca^{2+}, K_m was further reduced to 0.05 mM, but without an appreciable contribution of Na^+. At physiological concentrations of Na^+ and Ca^{2+}, the three HABP2 variants, and particularly G221E, displayed a major K_m increase for S-2288. Chemical footprinting revealed that Ile-16 is significantly less protected from chemical modification in G221E than in wild-type HABP2, suggesting impaired insertion of the N terminus into the G221E protease domain, with a concomitant impact on catalytic activity. Homology modeling suggested that the Glu-221 side chain could sterically hinder insertion of the N terminus into the HABP2 protease domain, helping to explain the detrimental effects of Glu-221 substitution on HABP2 activity.

HABP2 (hyaluronan-binding protein 2) is a Ca^{2+}-dependent protease that belongs to the family of serine proteases. The single-chain zymogen is activated by a single cleavage, resulting in a light chain consisting of the catalytic domain with the typical chymotrypsin fold and a heavy chain that comprises three EGF-like domains and a kringle domain (1, 2). HABP2 is also known as FSAP (factor seven-activating protease). This, however, proved to be a misnomer, because coagulation factor VII is a remarkably poor substrate for FSAP/HABP2 (3). In contrast, HABP2 does effectively activate single-chain urokinase-type plasminogen activator (scuPA),[2] suggesting a role in fibrinolysis (3–5). HABP2 has further been reported to cleave tissue-factor pathway inhibitor (6). Interestingly, HABP2/FSAP knockout mice display a mild bleeding phenotype, suggesting a role in hemostasis in relation to tissue-factor pathway inhibitor cleavage (7).

As a serine protease with the chymotrypsin fold, the protease domain of HABP2 contains a dual antiparallel β-barrel architecture (8, 9). In the β-barrel cleft resides the catalytic triad comprising the residues Ser-195, His-57, and Asp-102 (chymotrypsin numbering is used throughout this paper). In extension of the protein core, there are eight unique surface loops. These loops appear more variable between serine proteases because they are involved in substrate recognition and allosteric regulation of the catalytic activity. For instance, the so-called 70-loop of HABP2 may interact with Ca^{2+}, which is indispensable for allosteric regulation of the catalytic activity in coagulation factor IX and X (2, 10–12). In contrast, the 220-loop of thrombin, protein C, factor IX, and factor X is involved in Na^+ binding (13–16). The 220-loop is particularly important because it, together with the 180-loop, forms the primary S1 specificity pocket involved in recognition of the principle (P1) substrate residue (Arg in scuPA for HABP2). Moreover, the 220-loop is closely situated closely to the N terminus insertion pocket (8, 9).

Whether or not the 220-loop has similar implications in HABP2 remains unclear. The HABP2 220-loop is considerably shorter than that of the typical Na^+-binding proteases (see Fig. 7*A*). On the other hand, a polymorphism in the *HABP2* gene, which encodes the amino acid substitution G221E in the 220-loop (G534E in HABP2 numbering), has been associated with an increased risk for cardiovascular disease or venous thrombosis (17–19). This mutation has been designated as the Marburg I polymorphism and has been reported to cause reduced activity (17). Although the role of Gly-221 remains unclear, the above-mentioned findings indicate that G221E might not merely be a polymorphism and attributes a specific function to the 220-loop. In the present paper, we address the role of Gly-221 with particular reference to the regulation of HABP2 catalytic activity.

The authors declare that they have no conflicts of interest with the contents of this article.

[1] To whom correspondence should be addressed: Dept. of Plasma Proteins, Sanquin Research, Plesmanlaan 125, 1066 CX Amsterdam, The Netherlands. Tel.: 31-20-5123151; Fax: 31-20-5123310; E-mail: s.meijer@sanquin.nl.

[2] The abbreviations used are: scuPA, single-chain urokinase-type plasminogen activator; HGFA, hepatocyte growth factor activator; uPA, urokinase-type plasminogen activator.

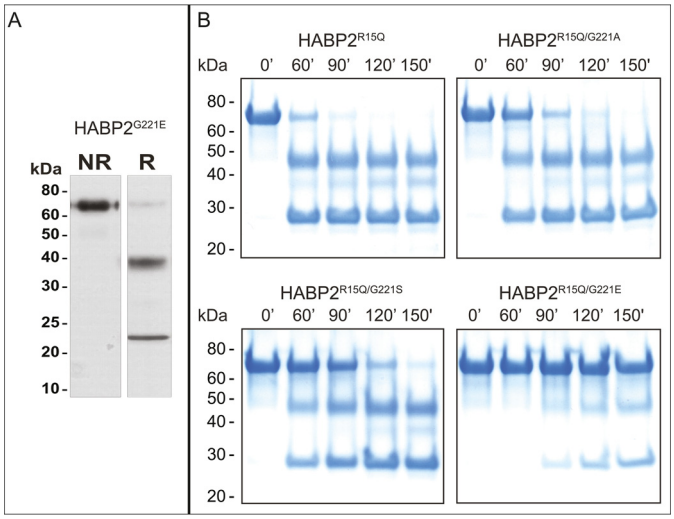

Figure 1. SDS-PAGE analysis of the HABP2 variants employed in this study. *A*, purified HABP2^{G534E} (1 μg/lane) was analyzed on 10% SDS-PAGE under reducing (*R*) and non-reducing (*NR*) conditions. Protein bands were visualized via silver staining. *B*, 0.7 μM HABP2^{R15Q}, HABP2$^{R15Q/G221A}$, HABP2$^{R15Q/G221S}$, and HABP2$^{R15Q/G221E}$ were incubated with 3 nM thermolysin for the indicated time intervals at 30 °C in 10 mM MES (pH 5.0), 150 mM NaCl, 5% (v/v) glycerol, 0.01% (v/v) Tween 80, 100 μM $CaCl_2$, and 50 nM $ZnCl_2$. Aliquots of the samples were separated on 4–12% SDS-PAGE, and the protein bands were visualized by Coomassie Brilliant Blue staining. The positions of the protein bands of the molecular mass markers are shown on the *left*.

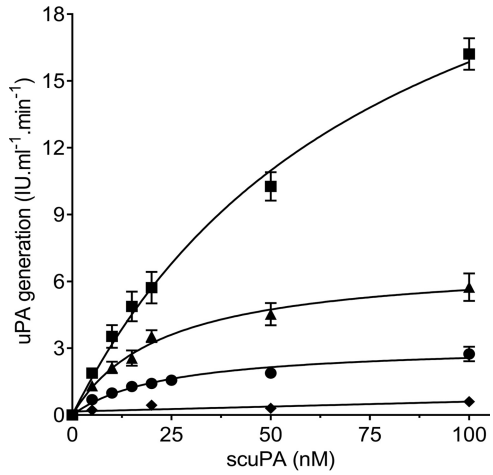

Figure 2. Activation of scuPA by the HABP2 variants. 0.25 nM of activated HABP2^{R15Q} (*squares*), HABP2$^{R15Q/G221A}$ (*triangles*), HABP2$^{R15Q/G221S}$ (*circles*), and HABP2^{G221E} (*diamonds*) were incubated with scuPA for 10 min at 37 °C in 100 mM NaCl, 0.1% (w/v) BSA, 0.01% (v/v) Tween 80, 5 mM $CaCl_2$, and 20 mM Tris-HCl (pH 7.5). Aprotinin was added to a final concentration of 125 nM to stop scuPA cleavage. The amount of generated uPA was measured employing S-2244 as described under "Experimental procedures." The data represent the means ± S.D. of at least three experiments.

Results

Construction of HABP2 derivatives

To elucidate the role of residue 221 for HABP2 function, we initially constructed three HABP2 variants in a WT-HABP2 background. In these variants, Gly-221 was replaced by either the small apolar alanine, the small polar serine, or the negatively charged glutamic acid. Protein expression studies revealed that HABP2^{G221A} and HABP2^{G221S} were, like WT-HABP2, highly sensitive to autocatalytic inactivation (data not shown). Purified HABP2^{G221E} was, however, fully processed into a two-chain form (Fig. 1*A*). N-terminal sequencing identified Ile-16 as the N terminus of the 25-kDa light chain, demonstrating that two-chain HABP2^{G221E} had been cleaved at the authentic activation site.

We have previously demonstrated that the inactivation of HABP2 can be controlled by mutating the natural site of activation into a cleavage site for the protease thermolysin (HABP2^{R15Q}) (3). We therefore constructed thermolysin cleavage sites in all the HABP2 variants. After introduction of this mutation, the variants were purified as a single-chain molecule. There was, however, a differential effect of thermolysin on these HABP2 derivatives. Whereas HABP2^{R15Q} was fully activated by thermolysin within 90 min, HABP2$^{R15Q/G221A}$ and HABP2$^{R15Q/G221S}$ required a prolonged incubation time with thermolysin to obtain the two-chain molecule. An even longer incubation with thermolysin was required to proteolytically process HABP2$^{R15Q/G221E}$. However, this also led to additional cleavages within the light chain of this variant. We were therefore unable to obtain two-chain HABP2$^{R15Q/G221E}$ (Fig. 1*B*). These observations show that the nature of the amino acid at position 221 affects the activation of the HABP2 variants by thermolysin. To examine the role of amino acid substitution at 221, we employed in this study HABP2$^{R15Q/G221S}$, HABP2$^{R15Q/G221A}$, and HABP2^{R15Q}, which can be specifically activated by thermolysin, as well as the constitutively active HABP2^{G221E}.

HABP2 activity toward macromolecular substrate scuPA

Each HABP2 variant was incubated with increasing concentrations of scuPA. The amount of uPA generated after 10 min was assessed employing the uPA-specific substrate S-2444 (Glu-Gly-Arg–*p*-nitroanilide). The data revealed that there is no detectable cleavage of scuPA in the presence of HABP2^{G221E} under these conditions (Fig. 2). HABP2$^{R15Q/G221A}$ and HABP2$^{R15Q/G221S}$ displayed slower scuPA activation than HABP2^{R15Q}. The data in Fig. 2 suggest that these mutants display a combination of lower K_m and k_{cat}, making the net effect on catalytic efficiency activity relatively small (see Table 2). Nevertheless, these data point to the possibility of changes in scuPA binding to HABP2 associated with mutations in position 221.

Effect of Na^+ on HABP2^{R15Q} activity in the presence and absence of Ca^{2+}

The catalytic activity of HABP2^{R15Q} toward the peptide substrate S-2288 (Ile-Pro-Arg–*p*-nitroanilide) was assessed at varying Na^+ concentrations in the presence or absence of Ca^{2+} (Fig. 3). In the absence of Ca^{2+}, the activity of HABP2^{R15Q} increased with increasing Na^+ concentrations (Fig. 3*A*). However, the effect of Na^+ was small in the presence of Ca^{2+} (Fig. 3*B*). Calculation of kinetic parameters showed that Na^+ causes a 5-fold drop in K_m in the absence of Ca^{2+}, whereas K_m proved independent of Na^+ when Ca^{2+} was present (Fig. 3*C*). As summarized in Table 1, Na^+ and Ca^{2+} did predominantly affect K_m, but not k_{cat}. In terms of catalytic efficiency (k_{cat}/K_m), Na^+ stimulated HABP2 activity by 5-fold, whereas the effect of Ca^{2+} was 8-fold higher (Table 1). Thus, in comparison with the

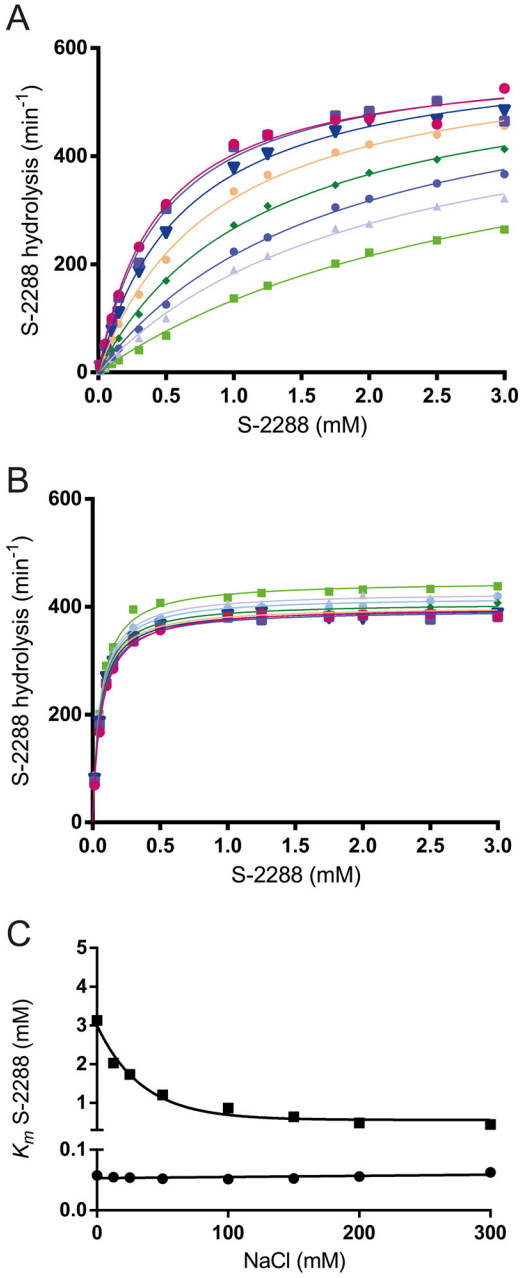

Figure 3. Effects of Na^+ and Ca^{2+} on S-2288 hydrolysis by activated HABP2^{R15Q}. *A*, displayed are the hydrolysis rates at varying concentrations of Na^+ in the absence of Ca^{2+}. S-2288 substrate conversion was assessed by incubation of 10 nM of activated HABP2^{R15Q} at 37 °C in 50 mM Tris-HCl (pH 8.0), 5 mM EDTA, and 0.1% (v/v) Tween 80. Na^+ concentrations are 0 mM (*green squares*), 12.5 mM (*light blue triangles*), 25 mM (*blue circles*), 50 mM (*green diamonds*), 100 mM (*light orange circles*), 150 mM (*blue inverted triangles*), 200 mM (*purple squares*), and 300 mM (*pink circles*). Choline chloride was used to maintain the ionic strength at 0.3 M. The data represent mean values of three experiments; S.D. values were below 10% of the mean. *B*, using the same experimental set-up, S-2288 hydrolysis was assessed at varying concentrations of Na^+ in the presence of 5 mM Ca^{2+} instead of 5 mM EDTA. *C*, calculated K_m values of HABP2^{R15Q} toward S-2288 either in absence (*squares*) or presence (*circles*) of 5 mM Ca^{2+}.

magnitude of the effect of Ca^{2+}, the effect of Na^+ seems limited. Control experiments (data not shown) indicated that in the absence of Ca^{2+}, Li^+ had no effect on the amidolytic activity of HABP2. The same holds for choline chloride, which was used to keep the ionic strength constant in the Na^+-titration studies.

Table 1
Effects of Na^+ and Ca^{2+} on S-2288 hydrolysis
The table below displays the kinetic constants of HABP2^{R15Q} for hydrolysis of S-2288 in either the presence or the absence of Na^+ and Ca^{2+}. The constants were obtained from fitting the data of Fig. 3 using the Michaelis-Menten equation.

Na^+ (150 mM)	Ca^{2+} (5 mM)	K_m	$10^{-2} \times k_{cat}$	$10^{-2} \times (k_{cat}/K_m)$
		mM	*min*$^{-1}$	*min*$^{-1}$ *mM*$^{-1}$
−	−	3.13 ± 0.3	5.5 ± 0.3	1.8
+	−	0.64 ± 0.05	6.0 ± 0.1	9.4
−	+	0.06 ± 0.03	4.5 ± 0.3	75.0
+	+	0.05 ± 0.02	4.0 ± 0.2	79.2

Amidolytic activity of the HABP2 variants

The activity of HABP2 variants was examined by Na^+- and Ca^{2+}-titration experiments. The activity of the mutants was dependent on the amino acid in position 221, in the order Gly > Ala > Ser > Glu (Fig. 4, *A* and *B*). Like HABP2^{R15Q}, increasing Na^+ concentrations enhanced the activity of the HABP2 variants (Fig. 4, *A* and *C*). Similarly, all variants displayed similar response to Ca^{2+} in the presence of Na^+ (Fig. 4, *B* and *D*), the optimal rate of substrate hydrolysis being reached at ~1 mM for all variants.

The kinetic parameters for S-2288 hydrolysis were then assessed in the presence of 5 mM $CaCl_2$ and 150 mM NaCl (Fig. 5 and Table 2). These data show that replacement of Gly in position 221 greatly reduces the catalytic efficiency. The most affected variant was HABP2$^{R15Q/G221E}$, which proved 400-fold less efficient than HABP2^{R15Q}. Because substitution of Gly-221 predominantly affects K_m, these data are compatible with perturbation of the interaction between active site of HABP2 and the substrate S-2288. Thus, Gly-221 in the 220-loop is beneficial for HABP2 activity toward both the peptide substrate S-2288 and the macromolecular substrate scuPA (Table 2).

Insertion of Ile-16 in the protease domain of HABP2^{G221E}

Following proteolytic activation of HABP2^{R15Q} and HABP2^{G221E}, insertion of the newly formed N terminus (Ile-16) was probed by incubating with sulfo-NHS-LC-biotin that specifically reacts with free, solvent-exposed amino groups (20, 21). The biotinylated proteins were proteolytically processed with trypsin and analyzed by mass spectrometry. After 5 min of incubation with sulfo-NHS-LC-biotin, a biotinylated N-terminal peptide of HABP2 was identified (*i.e.* biotin-IYGGFK, *m*/*z* 512.271) for both activated HABP2^{R15Q} and activated HABP2^{G221E}. The area under the curve of the reconstructed ion chromatograms shows that the degree of biotinylation at Ile-16 was at each time point higher for HABP2^{G221E} than for HABP2^{R15Q} (Fig. 6).

Discussion

The aim of the present study was to address the role of Gly-534 in the serine protease HABP2, and in particular the functional implication of the G534E substitution. This naturally occurring variant is encoded by the Marburg I polymorphism in the *HABP2* gene and has been associated with increased cardiovascular risk. In chymotrypsin numbering, the Marburg I polymorphism affects position 221 and thus is part of the characteristic 220-loop that participates in allosteric regulation of the catalytic activity in a variety of serine proteases (13–16, 22).

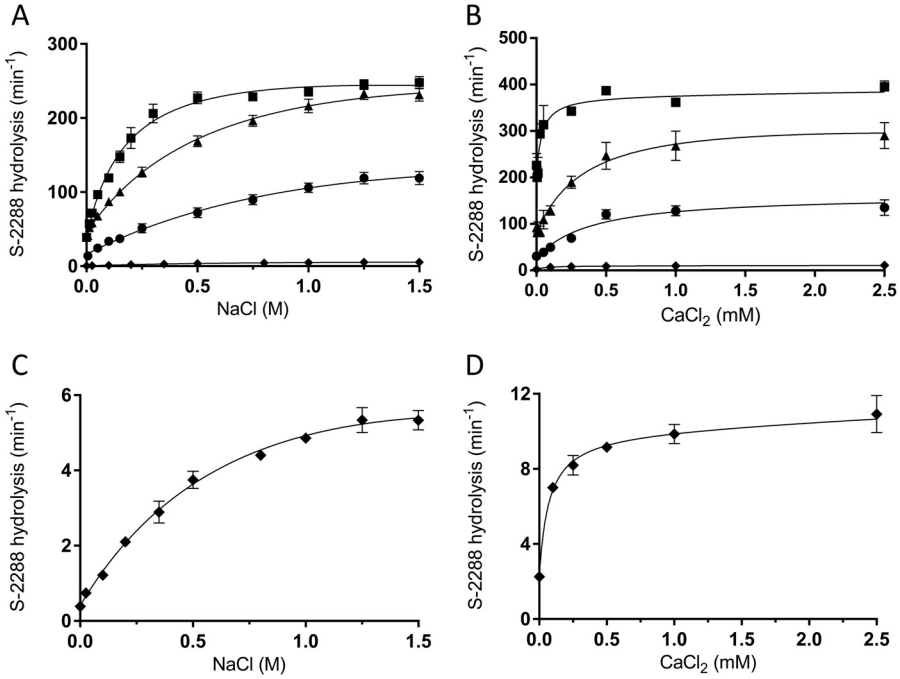

Figure 4. Effects of Na^+ and Ca^{2+} on S-2288 hydrolysis by HABP2 variants. *A*, the effect of Na^+ on the activity of the HABP2 derivatives is shown in the absence of Ca^{2+}. 17.5 nM of activated $HABP2^{R15Q}$ (*squares*), $HABP2^{R15Q/G221A}$ (*triangles*), $HABP2^{R15Q/G221S}$ (*circles*), and 350 nM of $HABP2^{G221E}$ (*diamonds*) were incubated with varying concentrations of NaCl at 37 °C in 50 mM Tris-HCl (pH 8.0), 5 mM EDTA, and 0.1% (v/v) Tween 80. Choline chloride was added to keep the salt concentration constant at 1.5 M. S-2288 was added to a final concentration of 625 μM, and its hydrolysis was assessed as described under "Experimental procedures." *B*, the effect of Ca^{2+} on the activity of the HABP2 variants. 17.5 nM of activated $HABP2^{R15Q}$ (*squares*), $HABP2^{R15Q/G221A}$ (*triangles*), $HABP2^{R15Q/G221S}$ (*circles*), and 350 nM of $HABP2^{G221E}$ (*diamonds*) were incubated with varying concentrations of $CaCl_2$ in 150 mM NaCl, 50 mM Tris-HCl (pH 8.0), 0.1% (v/v) Tween 80. *C* and *D*, separate graphs are given to better display titration curves for $HABP2^{G221E}$.

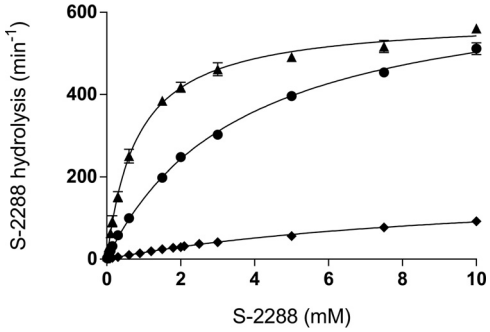

Figure 5. Hydrolysis of S-2288 by the HABP2 derivatives. 17.5 nM $HABP2^{R15Q/G221A}$ (*triangles*), 35 nM $HABP2^{R15Q/G221S}$ (*circles*), and 70 nM $HABP2^{G221E}$ (*diamonds*) were incubated with different concentrations of S-2288 at 37 °C in 50 mM Tris-HCl (pH 8.0), 150 mM NaCl, 5 mM $CaCl_2$, and 0.1% (v/v) Tween 80. The amount of cleaved S-2288 was measured as described under "Experimental procedures." The data represent the means ± S.D. of at least three experiments.

Table 2

Effects of Gly-221 substitutions on scuPA activation and S-2288 hydrolysis

Given are the calculated kinetic constants of the HABP2 variants for the proteolytic cleavage of scuPA and hydrolysis of S-2288. These constants were obtained by fitting data of Figs. 2, 3, and 5, respectively, to the Michaelis-Menten equation. Because of the low activity of $HABP2^{G221E}$ towards scuPA, kinetic constants thereof could not be determined (ND).

	Hydrolysis of S-2288			Activation of scuPA	
	K_m	$10^{-2} \times k_{cat}$	$10^{-2} \times (k_{cat}/K_m)$	V_{max}	K_m
	mM	min^{-1}	$min^{-1}\ mM^{-1}$	$IU\ ml^{-1}\ min^{-1}$	nM
$HABP2^{R15Q}$	0.05 ± 0.02	4.0 ± 0.2	79.2	28 ± 3	80 ± 16
$HABP2^{R15Q/G221A}$	0.8 ± 0.03	5.9 ± 0.1	8.5	6.9 ± 0.6	23 ± 5
$HABP2^{R15Q/G221S}$	3.7 ± 0.1	6.8 ± 0.1	2.5	3.2 ± 0.3	24 ± 5
$HABP2^{G221E}$	10 ± 0.4	1.8 ± 0.1	0.2	ND	ND

This raised the possibility that this loop, and in particular residue 221 therein, would serve a similar role in HABP2.

In related serine proteases such as activated protein C, factor IXa, and factor Xa, allosteric regulation involves interplay between the S1 site in the specificity pocket, the Ca^{2+}-binding site in the protease domain, and Na^+ binding that involves the 220-loop (14–16). In HABP2, the 220-loop differs from that in other mammalian serine proteases, in that it is two amino acid residues shorter (Fig. 7*A*). Moreover, HABP2 has Pro in position 225, which is typical for trypsin-like proteases, whereas most Na^+-binding serine proteases have Tyr in this position (22). In view of these differences, it is surprising that the amidolytic activity of activated HABP2 is sensitive not only to Ca^{2+}, but also to Na^+ (Figs. 3 and 4). The catalytic efficiency (k_{cat}/K_m) was ~5-fold increased by Na^+ alone and 42-fold by Ca^{2+} alone (Table 1). In the presence of Ca^{2+}, the contribution of Na^+ proved virtually absent, presumably because it is small in comparison with the Ca^{2+} response (Fig. 3*B* and Table 1). In this regard, HABP2 differs from for instance factor IXa, wherein Na^+ and Ca^{2+} contribute to a similar extent (14), or activated protein C, wherein the Na^+ response predominates (15). The limited response to Na^+ in the presence of Ca^{2+} makes it difficult to conclude whether or not HABP2, like activated protein C, factor IXa, and factor Xa (14–16), displays any thermodynamic linkage between the putative Na^+- and the Ca^{2+}-binding sites. It is evident, however, that Na^+ induces a 5-fold reduction of K_m for the peptide substrate S-2288 (Fig. 3*C*). Because k_{cat} remains essentially unchanged, the drop in K_m suggests that Na^+ substantially facilitates the interaction of HABP2 with the peptide substrate. This effect seems negligible, however, in the

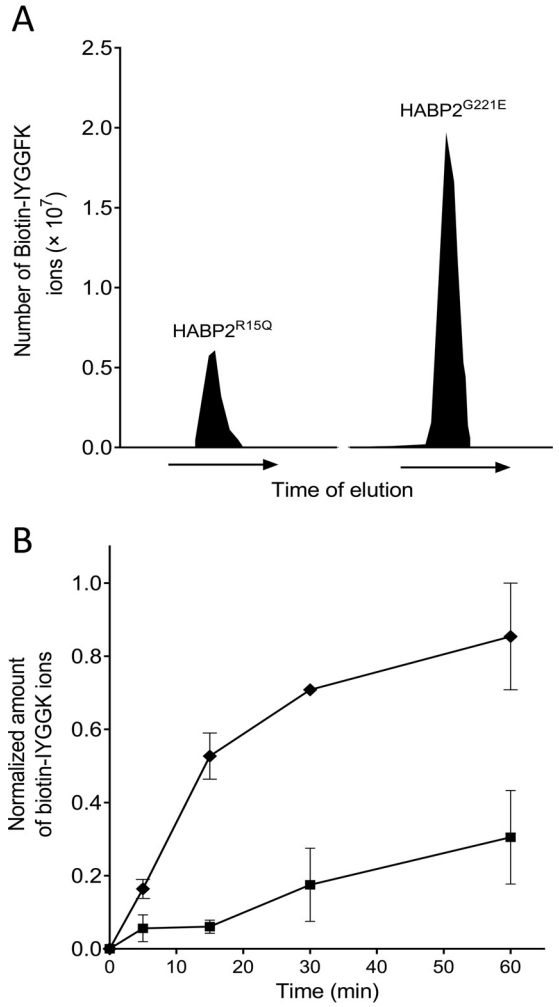

Figure 6. Reduced protection from chemical modification of the amino group of Ile-16 in HABP2^{G221E}. HABP2^{R15Q} and HABP2^{G221E} were incubated with sulfo-NHS-LC-biotin for different periods of time. Peptides of the HABP2 derivatives were obtained and separated on a C18 liquid chromatography column that was connected to a mass spectrometer as described under "Experimental procedures." *A*, shown are the reconstructed ion chromatograms of the eluted peptide representing the modified N terminus of HABP2^{R15Q} and of HABP2^{G221E} after 15 min of incubation with sulfo-NHS-LC-biotin. *B*, shown are the total number of modified N-terminal peptide ions of HABP2^{R15Q} (*squares*) and HABP2^{G221E} (*diamonds*) normalized to the maximum number of modified ions that were obtained for HABP2^{G221E} after 60 min of incubation with sulfo-NHS-LC-biotin (see "Experimental procedures"). The data show the averages of two independent experiments. The *error bars* show the deviation between the two experiments.

presence of Ca^{2+}, which reduces K_m by a further 12-fold (Fig. 3*B*). The Na^+ sensitivity of HABP2 implies that it is a Na^+-binding protease, in a manner that is highly reminiscent to related serine proteases that display Na^+ binding to the 220-loop. Because the effect of Na^+ is no longer apparent at physiological Ca^{2+} concentrations (Fig. 3*C* and Table 1), this is unlikely to be of physiological significance. In this respect HABP2 may be classified as being Na^+-*binding* but not Na^+-*dependent* in the strict sense.

As for the role of Gly in position 221, it is evident that the substitution into Ala or Ser leads to a moderate reduction of proteolytic activity of HABP2 toward scuPA, whereas mutation into Glu, the Marburg I variant, displays by far the most prominent defect (Fig. 2 and Table 2). Similar conclusions can be drawn with respect to amidolytic activity toward S-2288 (Fig. 5), although in terms of catalytic efficiency, the difference between mutants seems more pronounced (Table 2). The G221A and G221S substitutions predominantly increased K_m, which seems indicative for perturbed substrate interaction, whereas the effect of the G221E variant seems more complex, affecting both K_m and k_{cat}. We considered the possibility that the substitutions may severely affect the response to Na^+ and Ca^{2+}, but titration experiments did not provide any appreciable evidence in this direction (Fig. 4). Thus, the severely impaired activity of HABP2^{G221E} is unlikely to be due to a major disruption in the interaction between the S1 specificity pocket and the binding sites for Na^+ and/or Ca^{2+}. Another interaction with the S1 pocket in serine proteases occurs upon proteolytic activation via an electrostatic interaction between Asp-194 and the nascent new N terminus Ile-16 (9). The observation that in HABP2^{G221E} the N terminus is significantly more exposed than in normal HABP2 (Fig. 6) suggests that HABP2^{G221E} lacks the stabilization of the S1 pocket that normally results from N terminus insertion. As such, the activated form of HABP2^{G221E} may predominantly be inactive, presumably because of a shift of the equilibrium between closed (E*) and open (E) forms (23) or in the continuum between zymogen- and proteinase-like states (24).

In absence of a crystal structure of HABP2, it remains difficult to fully appreciate the role of Gly-221 and the effect of the mutations described in the present paper. Of all human serine proteases, hepatocyte growth factor activator (HGFA) exhibits the highest primary sequence homology with full-length HABP2 (1). To assess the structural role Gly-221, we constructed a model of the catalytic domain of HABP2 based on that of HGFA by employing comparative homology modeling (25, 26). Fig. 7*B* shows the structure of the active site region of HABP2, with the putative position of the Ca^{2+} and Na^+ ions. As for Na^+-binding, five of six coordinating ligands could be provided by the carbonyl O-atoms of residues Gly-221, Lys-221a, and Arg-224 from the 220-loop and Leu-185 and Asn-185a from the opposite 180-loop (Fig. 7*B*). Although in other Na^+-binding serine proteases, the coordination for Na^+ binding is disrupted by Pro in position 225 (22), HABP2 may be an exception because its 220-loop is shorter and thereby less sensitive to destabilization by the side chain at position 225. The model suggests that in HABP2^{G221E} the putative Na^+ coordination may be conserved (Fig. 7*C*), which seems compatible with the observed Na^+ response of this variant (Fig. 4*C*). The model further suggests that Glu in position 221 could introduce a steric clash with Tyr-17, thus impeding the insertion of the new N terminus Ile-16 after HABP2 activation (Fig. 7*C*) and the concomitant conversion of the zymogen-like form into the proteinase-like conformation.

The findings of this study show that Gly-221 is of major importance for the catalytic activity of HABP2. As such, the significance of position 221 is shared with other serine proteases like protein C, factor IX, and thrombin. For thrombin, mutation of the Asp-221 into a glutamic acid, which is highly similar in properties to the former amino acid residue, already leads to a severe defect in fibrinogen clotting (27). Similarly, the G221R mutation in protein C leads to an impaired biological

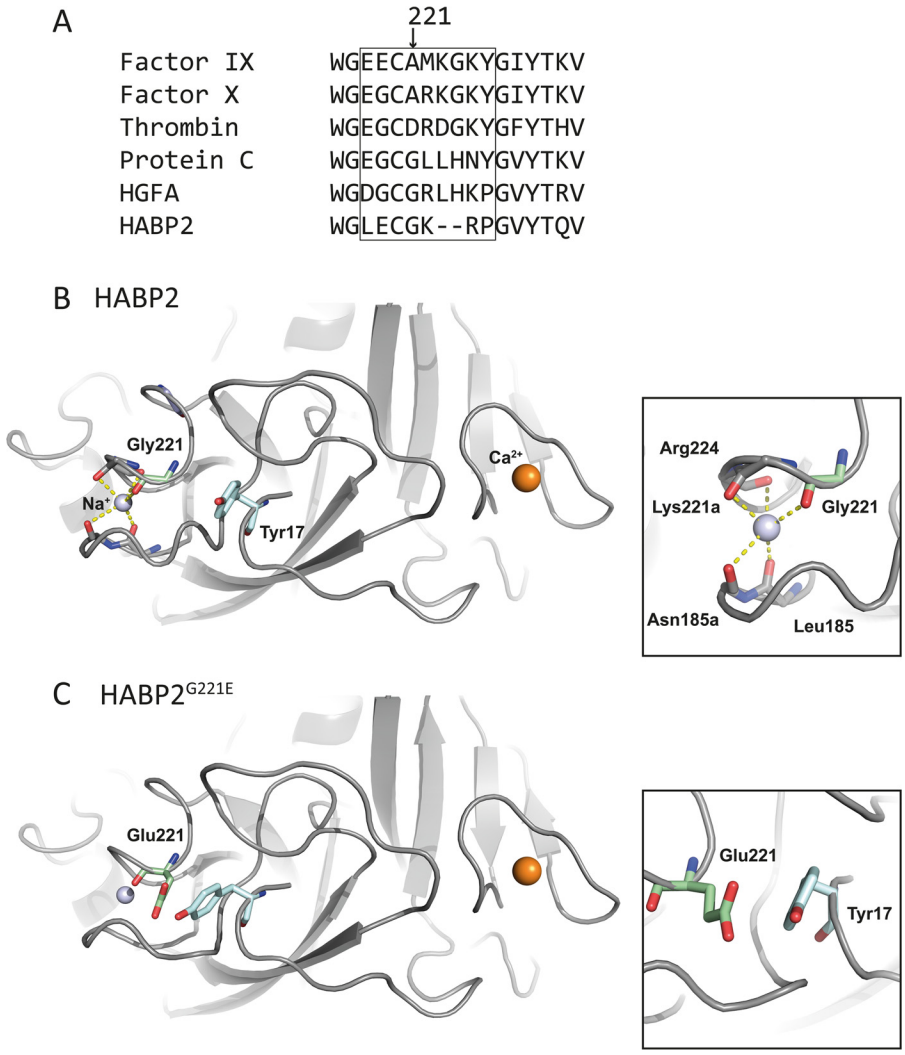

Figure 7. Position 221 in the HABP2 protease domain. *A*, the 220-loop (delineated by a *box*) of HABP2 is shorter than that of other serine proteases as visualized by the primary sequence alignment. Except for Cys-220, the 220-loop residues of HABP2 are poorly conserved with those of factor IX, X, thrombin, and protein C. *B*, models of the HABP2 protease domain were constructed with Modeler 9v7 employing the crystal structure of HGFA as a template (Protein Data Bank code 1YC0) (26). The presence of the Na^+ ion was modeled according to its position in the FXa crystal structure (Protein Data Bank code 2BOK) (32). A representative image is shown that also comprises the Ca^{2+}-binding site, 220-loop, S1 pocket, and N terminus insertion site. The modeled Na^+ ion is shown as a *light blue sphere*, and the Ca^{2+} ion is shown as an *orange sphere*. A close-up is given of the 180-loop and 220-loop in interaction with a Na^+ ion. Putative coordination of the Na^+ ion by amino acid carbonyl groups of Leu-185, Asn185-a, Gly-221, Lys-221a, and Arg-224 is indicated by *dashed lines*. Tyr-17 at the N terminus of the protease domain is indicated in *cyan*, and Gly-221 is shown in a *green*-colored stick representation. *C*, the model of $HABP2^{G221E}$ displays the potential steric and electrostatic repulsion between Glu-221 and Tyr-17 at the N terminus insertion site. On the right, a close-up is shown of Glu-221 and Tyr-17 in respectively *green*- and *cyan*-colored stick representations. All images were generated using PyMOL (Schrödinger).

activity of this protease (28). In contrast, alanine to aspartic acid exchange in coagulation factor IX does not affect its clotting activity or its binding to macromolecular substrates at all (29). However, mutation of the same alanine into a valine severely impairs activity, which has been attributed to obstruction of N terminus insertion by the branched side chain (29). Our study proposes a similar role of position 221 in the 220-loop on N terminus insertion in HABP2.

In view of the numerous substrates that have been proposed for HABP2 (3–7, 10), it remains difficult to predict the phenotype associated with Gly-221 substitution. It remains plausible that HABP2 is a promiscuous enzyme that activates more substrates than scuPA alone and thus may have more roles than stimulation of fibrinolysis. However, irrespective of the physiological function of HABP2, it is evident that the G221E substitution as encoded by the Marburg I polymorphism results in a severely dysfunctional protein.

Experimental procedures

Chemicals

All chemical were from Sigma-Aldrich unless otherwise stated. Sulfo-NHS-LC-biotin was from QB Perbio (Tattenhall, Cheshire, UK). Acetonitrile and ultra-pure water, which were employed for mass spectrometry, were obtained from Biosolve (Valkenswaard, The Netherlands).

Recombinant HABP2 derivatives and their activation by thermolysin

Recombinant $HABP2^{R15Q}$ is described by Stavenuiter *et al.* (3). The thermolysin HABP2 variants carrying amino acid

substitution at position 221 were constructed employing QuikChange mutagenesis (Stratagene, La Jolla, CA) using HABP2^{R15Q} DNA as a template and the appropriate primers. Recombinant proteins were produced, purified, activated, and quantified as described (3). The HABP2 variants were activated by incubating 0.7 μM of the protein with 3 nM thermolysin for 2 h at 30 °C in buffer containing 10 mM MES (pH 5.0), 150 mM NaCl, 5% (v/v) glycerol, 0.01% (v/v) Tween 80, 100 μM $CaCl_2$, and 50 nM $ZnCl_2$. Thermolysin was inhibited by the addition of phosphoramidon disodium salt to a final concentration of 10 μM. Because of its inherent instability, HABP2 was freshly activated for all individual experiments. SDS/PAGE was performed to check whether activation was complete (>90–95%). Molar concentrations of activated HABP2 were based on protein concentrations prior to activation.

Hydrolysis of S-2288 by HABP2 derivatives and the determination of uPA concentration

The initial rates of *p*-nitroaniline release from S-2288 were measured by following the absorbance at 405 nm using a Rosys-Anthos Lucy 3 photometer (Anthos Labtec Instruments GmbH, Wals, Austria). To calculate the concentration of *p*-nitroaniline, an extinction coefficient of 9.9 mM^{-1} cm^{-1} was used. The concentration of uPA, obtained from scuPA cleavage by the HABP2 derivatives, was assessed by adding S-2444 to the reaction mixture (final concentration, 375 μM) (3). The initial rates of *p*-nitroaniline release were assessed by monitoring the absorbance at 405 nm in time as described above. The results were corrected for the background levels of *p*-nitroaniline in the absence of the HABP2 derivatives. Absorbance changes were converted into increase in *p*-nitroaniline concentration and divided by the enzyme concentration to yield S-2288 hydrolysis rates in min^{-1}. The concentration of uPA was determined using a calibration curve of the HMW uPA international standard 87/594 (National Institute for Biological Standards and Control (NIBSC), South Mimms, UK).

Determination of steady states kinetic constants and inhibition kinetics

Kinetic constants of S-2288 hydrolysis and scuPA activation by the HABP2 derivatives were assessed by assuming Michaelis-Menten-like behavior for the enzymatic reactions (30). GraphPad software was employed to fit the data to the Michaelis-Menten equation employing non-linear regression.

Biotinylation of the free amino group of Ile-16

350 nM of activated HABP2^{R15Q} or HABP2^{G221E} was incubated with 25 mM sulfo-NHS-biotin in 100 mM NaCl, 1 mM $CaCl_2$, 0.02% (v/v) Tween 80, 50 mM HEPES (pH 7.5). At different time points, the reactions were stopped by the addition of lysine (125 mM). Proteins were subsequently separated on precast NuPage 4–12% Bis-Tris gels (Invitrogen) under reducing conditions. The protein bands were subsequently visualized employing Coomassie Brilliant Blue staining. Bands of interest were excised and processed for in-gel digestion according to the method of Shevchenko et al. (31). Briefly, the bands were washed with a buffer containing 50 mM ammonium bicarbonate (pH 7.9) followed by a wash with 50% (v/v) acetonitrile. This step was repeated three times. Cysteine bonds were subsequently reduced with 10 mM dithiothreitol for 1 h at 56 °C and alkylated with 50 mM iodoacetamide for 45 min at room temperature in the dark. After two subsequent wash/dehydration cycles, the bands were dried for 10 min in a vacuum centrifuge (Thermo Fisher Scientific Inc.) and incubated overnight with 0.06 μg/μl trypsin at 37 °C. Peptides were eluted from the gel with 1% (v/v) formic acid and twice with 50% (v/v) acetonitrile and 5% (v/v) formic acid. The three elution fractions were pooled and concentrated to 20 μl in a vacuum centrifuge.

Mass spectrometry and data analysis

The above-described peptides were separated using a reversed-phase C18 column (50 μm × 40 cm, 5-μm particles) (Nanoseparations, Nieuwkoop, The Netherlands) running at 100 nl/min with a 1-h gradient from 0% to 35% (v/v) acetonitrile with 0.1% (v/v) acetic acid. The peptides were sprayed directly from the column into the LTQ Orbitrap mass spectrometer (Thermo Fisher Scientific Inc.) using a nanoelectrospray source with a spray voltage of 1.9 kV. The LTQ was operated in a data-dependent mode by performing collision induced dissociation in the ion trap (35% normalized collision energy) for the five most intense precursor ions selected from each full scan in the Orbitrap (350–2000 m/z, resolving power 30.000). An isolation width of 2 Da was used for the selected ions (charge ≥ 2) and an activation time of 30 ms. Dynamic exclusion was activated for the MS/MS scan with a repeat count of 1 and exclusion duration of 30 s. Peptides were identified employing a Sequest search against the human entries in the NCBI database utilizing Proteome Discoverer 1.0 software (Thermo Scientific). The same software was used to obtain the peak area of the reconstructed ion chromatograms of the peptide precursor ions for quantification purposes. Direct comparison of the tryptic digests obtained from gel is not possible because of a differential loss of the peptides during the peptide purification procedure. Therefore, the areas of the reconstructed ion chromatograms of control peptides present in each sample were used as a reference to correct for peptide loss.

Author contributions—F. S. constructed and purified the HABP2 variants and performed and analyzed the experiments. E. H. T. M. E. constructed the HAPB2 models. F. S., E. H. T. M. E., K. M., and A. B. M. wrote the manuscript. All authors reviewed the results and approved the final version of the manuscript.

References

1. Choi-Miura, N. H., Tobe, T., Sumiya, J., Nakano, Y., Sano, Y., Mazda, T., and Tomita, M. (1996) Purification and characterization of a novel hyaluronan-binding protein (PHBP) from human plasma: it has three EGF, a kringle and a serine protease domain, similar to hepatocyte growth factor activator. *J. Biochem.* **119,** 1157–1165
2. Hunfeld, A., Etscheid, M., König, H., Seitz, R., and Dodt, J. (1999) Detection of a novel plasma serine protease during purification of vitamin K-dependent coagulation factors. *FEBS Lett.* **456,** 290–294
3. Stavenuiter, F., Dienava-Verdoold, I., Boon-Spijker, M. G., Brinkman, H. J., Meijer, A. B., and Mertens, K. (2012) Factor seven activating protease (FSAP): does it activate factor VII? *J. Thromb. Haemost.* **10,** 859–866
4. Choi-Miura, N. H., Yoda, M., Saito, K., Takahashi, K., and Tomita, M. (2001) Identification of the substrates for plasma hyaluronan binding protein. *Biol Pharm Bull.* **24,** 140–143

5. Römisch, J., Vermöhlen, S., Feussner, A., and Stöhr, H. (1999) The FVII activating protease cleaves single-chain plasminogen activators. *Haemostasis* **29,** 292–299
6. Kanse, S. M., Declerck, P. J., Ruf, W., Broze, G., and Etscheid, M. (2012) Factor VII-activating protease promotes the proteolysis and inhibition of tissue factor pathway inhibitor. *Arterioscler. Thromb. Vasc. Biol.* **32,** 427–433
7. Subramaniam, S., Thielmann, I., Morowski, M., Pragst, I., Sandset, P. M., Nieswandt, B., Etscheid, M., and Kanse, S. M. (2015) Defective thrombus formation in mice lacking endogenous factor VII activating protease (FSAP). *Thromb. Haemost.* **113,** 870–880
8. Di Cera, E. (2009) Serine proteases. *IUBMB Life* **61,** 510–515
9. Page, M. J., and Di Cera, E. (2008) Serine peptidases: classification, structure and function. *Cell Mol. Life Sci.* **65,** 1220–1236
10. Kannemeier, C., Feussner, A., Stöhr, H. A., Weisse, J., Preissner, K. T., and Römisch, J. (2001) Factor VII and single-chain plasminogen activator-activating protease: activation and autoactivation of the proenzyme. *Eur J Biochem.* **268,** 3789–3796
11. Mathur, A., Zhong, D., Sabharwal, A. K., Smith, K. J., and Bajaj, S. P. (1997) Interaction of factor IXa with factor VIIIa: effects of protease domain Ca^{2+} binding site, proteolysis in the autolysis loop, phospholipid, and factor X. *J. Biol. Chem.* **272,** 23418–23426
12. Sabharwal, A. K., Padmanabhan, K., Tulinsky, A., Mathur, A., Gorka, J., and Bajaj, S. P. (1997) Interaction of calcium with native and decarboxylated human factor X: effect of proteolysis in the autolysis loop on catalytic efficiency and factor Va binding. *J. Biol. Chem.* **272,** 22037–22045
13. Pineda, A. O., Carrell, C. J., Bush, L. A., Prasad, S., Caccia, S., Chen, Z. W., Mathews, F. S., and Di Cera, E. (2004) Molecular dissection of Na^+ binding to thrombin. *J. Biol. Chem.* **279,** 31842–31853
14. Schmidt, A. E., Stewart, J. E., Mathur, A., Krishnaswamy, S., and Bajaj, S. P. (2005) Na^+ site in blood coagulation factor IXa: effect on catalysis and factor VIIIa binding. *J. Mol. Biol.* **350,** 78–91
15. Schmidt, A. E., Padmanabhan, K., Underwood, M. C., Bode, W., Mather, T., and Bajaj, S. P. (2002) Thermodynamic linkage between the S1 site, the Na^+ site, and the Ca^{2+} site in the protease domain of human activated protein C (APC): Sodium ion in the APC crystal structure is coordinated to four carbonyl groups from two separate loops. *J. Biol. Chem.* **277,** 28987–28995
16. Underwood, M. C., Zhong, D., Mathur, A., Heyduk, T., and Bajaj, S. P. (2000) Thermodynamic linkage between the S1 site, the Na^+ site, and the Ca^{2+} site in the protease domain of human coagulation factor Xa: Studies on catalytic efficiency and inhibitor binding. *J. Biol. Chem.* **275,** 36876–36884
17. Etscheid, M., Muhl, L., Pons, D., Jukema, J. W., König, H., and Kanse, S. M. (2012) The Marburg I polymorphism of factor VII activating protease is associated with low proteolytic and low pro-coagulant activity. *Thromb. Res.* **130,** 935–941
18. Ireland, H., Miller, G. J., Webb, K. E., Cooper, J. A., and Humphries, S. E. (2004) The factor VII activating protease G511E (Marburg) variant and cardiovascular risk. *Thromb. Haemost.* **92,** 986–992
19. Weisbach, V., Ruppel, R., and Eckstein, R. (2007) The Marburg I polymorphism of factor VII-activating protease and the risk of venous thromboembolism. *Thromb. Haemost.* **97,** 870–872
20. Gabant, G., Augier, J., and Armengaud, J. (2008) Assessment of solvent residues accessibility using three sulfo-NHS-biotin reagents in parallel: application to footprint changes of a methyltransferase upon binding its substrate. *J. Mass Spectrom.* **43,** 360–370
21. Azim-Zadeh, O., Hillebrecht, A., Linne, U., Marahiel, M. A., Klebe, G., Lingelbach, K., and Nyalwidhe, J. (2007) Use of biotin derivatives to probe conformational changes in proteins. *J. Biol. Chem.* **282,** 21609–21617
22. Dang, Q. D., and Di Cera, E. (1996) Residue 225 determines the Na^+-induced allosteric regulation of catalytic activity in serine proteases. *Proc. Natl. Acad. Sci. U.S.A.* **93,** 10653–10656
23. Vogt, A. D., Chakraborty, P., and Di Cera, E. (2015) Kinetic dissection of the pre-existing conformational equilibrium in the trypsin fold. *J. Biol. Chem.* **290,** 22435–22445
24. Kamath, P., Huntington, J. A., and Krishnaswamy, S. (2010) Ligand binding shuttles thrombin along a continuum of zymogen- and proteinase-like states. *J. Biol. Chem.* **285,** 28651–28658
25. Sali, A., and Blundell, T. L. (1993) Comparative protein modelling by satisfaction of spatial restraints. *J. Mol. Biol.* **234,** 779–815
26. Shia, S., Stamos, J., Kirchhofer, D., Fan, B., Wu, J., Corpuz, R. T., Santell, L., Lazarus, R. A., and Eigenbrot, C. (2005) Conformational lability in serine protease active sites: structures of hepatocyte growth factor activator (HGFA) alone and with the inhibitory domain from HGFA inhibitor-1B. *J. Mol. Biol.* **346,** 1335–1349
27. Rouy, S., Vidaud, D., Alessandri, J. L., Dautzenberg, M. D., Venisse, L., Guillin, M. C., and Bezeaud, A. (2006) Prothrombin Saint-Denis: a natural variant with a point mutation resulting in Asp to Glu substitution at position 552 in prothrombin. *Br. J. Haematol.* **132,** 770–773
28. Miyata, T., Zheng, Y. Z., Sakata, T., Tsushima, N., and Kato, H. (1994) Three missense mutations in the protein C heavy chain causing type I and type II protein C deficiency. *Thromb. Haemost.* **71,** 32–37
29. Hamaguchi, N., Roberts, H., and Stafford, D. W. (1993) Mutations in the catalytic domain of factor IX that are related to the subclass hemophilia Bm. *Biochemistry* **32,** 6324–6329
30. Segel, I. H. (1975) *Enzyme Kinetics: Behavior and Analysis of Rapid Equilibrium and Steady-state Enzyme Systems*, pp. 25–29, John Wiley & Sons, Inc., New York
31. Shevchenko, A., Tomas, H., Havlis, J., Olsen, J. V., and Mann, M. (2006) In-gel digestion for mass spectrometric characterization of proteins and proteomes. *Nat. Protoc.* **1,** 2856–2860
32. Schärer, K., Morgenthaler, M., Paulini, R., Obst-Sander, U., Banner, D. W., Schlatter, D., Benz, J., Stihle, M., and Diederich, F. (2005) Quantification of cation-pi interactions in protein-ligand complexes: crystal-structure analysis of factor Xa bound to a quaternary ammonium ion ligand. *Angew. Chem. Int. Ed. Engl.* **44,** 4400–4404

Role of glycine 221 in catalytic activity of hyaluronan-binding protein 2

Fabian Stavenuiter, Eduard H. T. M. Ebberink, Koen Mertens and Alexander B. Meijer

J. Biol. Chem. 2017, 292:6381-6388.
doi: 10.1074/jbc.M116.757849 originally published online February 27, 2017